Information flows from hippocampus to cortex during replay of verbal working memory items.

Vasileios Dimakopoulos[1], Lennart Stieglitz[1], Pierre Mégevand[2,3], Johannes Sarnthein[1,4*]

1 Klinik für Neurochirurgie, Universitätsspital Zürich, Universität Zürich, 8091 Zurich, Switzerland
2 Département des neurosciences fondamentales, Faculté de médecine, Université de Genève, Geneva, Switzerland
3 Service de neurologie, Hôpitaux Universitaires de Genève, Geneva, Switzerland
4 Neuroscience Center Zurich, ETH Zurich, 8092 Zurich, Switzerland

vasileios.dimakopoulos@usz.ch
lennart.stieglitz@usz.ch
pierre.megevand@unige.ch
johannes.sarnthein@usz.ch
*Correspondence should be addressed to J.S.

Keywords: Granger causality, phase-locking value, auditory cortex, posterior cortex, beta rhythm

ABSTRACT

Background: The maintenance of items in working memory (WM) relies on a widespread network of cortical areas and hippocampus where synchronization between electrophysiological recordings reflects functional coupling. We investigated the direction of information between sensory areas and hippocampus during encoding and maintenance of WM items.

Methods: Participants (N=15) performed a WM task where a string of letters was presented all at once, thus separating the encoding period from the maintenance period. Participants mentally replayed the letters during maintenance. We recorded sEEG from the hippocampus, scalp EEG and, additionally in 3 participants, temporo-parietal ECoG.

Results: When analyzing the information flow to and from auditory cortex by Granger causality, the flow was from ECoG over auditory cortex to hippocampus with a peak in the 12-24 Hz beta range while letters were presented, and this flow was subsequently reversed during maintenance, while letters were maintained in memory. The same pattern appeared to and from hippocampus with ECoG over temporo-parietal cortex. For scalp EEG, the pattern appeared on temporal sites, albeit in the 4-12 Hz theta-alpha range. While the pattern was significantly structured for correct trials, it was unstructured for incorrect trials.

Conclusions: The functional interaction between hippocampus and cortex and the reversal of information flow provide a physiological basis for the encoding of memory items and their active replay during maintenance.

SIGNIFICANCE STATEMENT

How do we encode and recall memories to guide action within seconds? Here, we investigated electrical activity in hippocampus and cortex while the participants mentally replayed a set of letters to maintain them working memory with the aim to respond correctly. We found clear evidence that during the encoding of the letters, the information flow was from sensory cortex to hippocampus (bottom-up). The flow was subsequently reversed during maintenance (top-down), thus providing a physiological basis for the recall of the memory items. This functional interaction provides the first evidence of bidirectional communication during encoding and the active replay of memory items.

INTRODUCTION

Working memory (WM) describes our capacity to represent sensory input for prospective use (1, 2). Maintaining content in WM requires collaboration within a widespread network of brain regions. The anatomical basis of WM was shown noninvasively with EEG / MEG (3-9) and invasively with intracranial EEG (10-19) and single unit recordings (19-22).

In cortical brain regions, WM maintenance correlates with sustained neuronal oscillations, most frequently reported in the theta-alpha range (4-12 Hz) (3, 5-7, 10, 11, 13, 19, 23). Also in the hippocampus, WM maintenance was associated with sustained theta-alpha oscillations (14, 19). As a hallmark for WM maintenance, persistent neuronal firing was reported during the absence of sensory input, indicating the involvement of the medial temporal lobe in WM (19-21).

At the network level, synchronized oscillations have been proposed as a mechanism for functional interactions between brain regions (24, 25). It is thought that these oscillations show temporal coupling of the low-frequency phase for long-range communication between cortical areas (4, 6, 13, 17-19, 26). This synchronization suggests an active maintenance process through reverberating signals between brain regions.

We here extend previous studies with the same task (3), which had shown parietal activation and strong scalp EEG synchronization between stereotactic EEG (sEEG) in the hippocampus and scalp EEG (19). In addition to scalp EEG and hippocampal sEEG, three participants of this study had cortical recordings (ECoG) from

77 electrodes over primary auditory, parietal and occipital cortical areas. Given the low
78 incidence of the epileptogenic zone in parietal cortex, parietal ECoG recordings are
79 rare. We found that the information flow was from sensory areas to hippocampus
80 during the encoding of WM items and the flow was from hippocampus to cortex for
81 the replay of the items during the maintenance period.

82 # RESULTS

83 ## Task and behavior

84 Fifteen participants (median age 29 y, range [18-56], 7 male) performed a
85 modified Sternberg WM task (71 sessions in total, 50 trials each). In the task, items
86 were presented all at once rather than sequentially, thus separating the encoding
87 period from the maintenance period. In each trial, the participant was instructed to
88 memorize a set of 4, 6 or 8 letters presented for 2 s (encoding). The number of
89 letters was thus specific for the memory workload. The participants read the letters
90 themselves and heard them spoken at the same time. After a delay (maintenance)
91 period of 3 s, a probe letter prompted the participant to retrieve their memory
92 (retrieval) and to indicate by button press ("IN" or "OUT") whether or not the probe
93 letter was a member of the letter set held in memory (**Fig. 1a**). During the
94 maintenance period, participants rehearsed the verbal representation of the letter
95 strings subvocally, i.e. mentally replayed the memory items. This activation of the
96 phonological loop (1) is a component of verbal WM as it serves to produce an
97 appropriate behavioral response (2).

98 The mean correct response rate was 91% (both for IN and OUT trials). The rate of
99 correct responses decreased with set size from a set size of 4 (97% correct
100 responses) to set sizes of 6 (89%) and 8 (83%) (**Fig. 1 b**). Across the participants,
101 the memory capacity averaged 6.1 (Cowan's K, (correct IN rate + correct OUT rate -
102 1)*set size), which indicates that the participants were able to maintain at least 6
103 letters in memory. The mean response time (RT) for correct trials (3045 trials) was
104 1.1 ± 0.5 seconds and increased with workload from set size 4 (1.1 ± 0.5 s) to 6 (1.2
105 ± 0.5 s) and 8 (1.3 ± 0.6 s), 53 ms/item (**Fig. 1 c**). Correct IN/OUT decisions were
106 made more rapidly than incorrect decisions (1.1 ± 0.5 versus 1.3 ± 0.6 seconds).
107 These data show that the participants performed well in the task and that the
108 difficulty of the trials increased with the number of letters in the set. In further

analysis, we focused on correct trials with set size 6 and 8 letters to assure hippocampal activation and hippocampo-cortical interaction as shown earlier (19).

Power spectral density in cortical and hippocampal recordings

To investigate how cortical and hippocampal activity subserves WM processing, we analyzed sEEG recorded in the hippocampus (**Fig. 1 d**) together with ECoG from cortical strip electrodes (**Fig. 2 a, Fig. 3 a, f**). In the following, we present power spectral density (PSD) time-frequency maps from representative electrode contacts.

In an occipital recording of Participant 1 (grid contact H3, **Fig. 2 a**), strong gamma activity (> 40 Hz) in the relative power spectral density (PSD) occurred while the participant viewed the letters during encoding (**Fig. 2 b**). After the letters disappeared from the screen, activity occurred in the beta range (12-24 Hz) towards the end of the maintenance period. In a temporal recording (grid contact C2) gamma activity occurred during encoding, thus confirming the anatomical localization of this contact over auditory cortex (supplementary **Fig. S1 a**). Similarly, the temporal scalp EEG of Participant 2 (electrode site T3, **Fig 3 a**) showed activity during encoding and maintenance, albeit at lower frequencies (**Fig 3 b**). In Participant 3, a similar pattern occurred in the PSD of a temporo-parietal recording (most anterior strip electrode contact, **Fig 3 f**), where the appearance of the probe letter again prompted gamma activity. This site coincides with the generator of scalp EEG that was found in the parietal cortex for the same task (3). The PSD thereby confirmed the findings of local synchronization of cortical activity during WM maintenance (3, 8, 9).

In the hippocampus of all three participants, we found elevated activity in the beta range (12-24 Hz) towards the end of the maintenance period (**Fig 2 c, Fig 3 c,h**), confirming the hippocampal contribution to processing of this task (19)

Directed functional coupling between hippocampus and ECoG

To investigate the functional coupling between cortex and hippocampus, we first calculated the phase locking value (PLV). During maintenance, we found enhanced PLV in the beta range (supplementary **Fig. S1 b**). The highest PLV occurred from the contact C2 over auditory cortex (**Fig 2 d**), which speaks for a functional coupling between auditory cortex and hippocampus mediated by synchronized oscillations (24).

What was the directionality of the information flow during encoding and maintenance in a trial? We used spectral Granger causality (GC) as a measure of

directed functional connectivity to determine the direction of the information flow between auditory cortex and hippocampus during the trials. During encoding, the information flow was from auditory cortex to hippocampus with a maximum in the beta frequency range (12-24 Hz, dark blue curve in **Fig. 2 e**). During maintenance, the information flow in the same frequency range was reversed (dark red curve), i.e. from hippocampus to auditory cortex. Concerning the spatial distribution of the beta GC, the highest GC during encoding occurred from auditory cortex to hippocampus (supplementary **Fig. S1 c**). During maintenance, the beta GC was high from hippocampus to both auditory cortex and parietal cortex (supplementary **Fig. S1 d**). As a further illustration of the GC time-course, the time-frequency plot shows the difference between GC spectra (ΔGranger) at each time point, where blue indicates net flow from auditory cortex to hippocampus and red indicates net flow from hippocampus to auditory cortex **Fig. 2 f**).

Similarly in Participant 2, the time course of GC followed the same pattern between auditory cortex (anterior strip electrode contact in **Fig. 3 a**) and hippocampus (**Fig. 3 d,e**). Among all participants that had both sEEG and temporo-parietal ECoG recordings, Participant 3 had an electrode contact over visual cortex; the sensory localization was indexed by the strong gamma activity (most posterior contact of the strip electrode in **Fig. 3 f**). The time-course of information flow between visual cortex and hippocampus (**Fig. 3 i,j**) followed the same pattern as described for the auditory cortex above. Thus, letters were encoded with information flow from sensory cortex to hippocampus; conversely, the information flow from hippocampus to sensory cortex indicated the replay of letters during maintenance.

Directed functional coupling between hippocampus and scalp EEG

We then confirmed the directed functional coupling in the whole group of N = 15 participants. We calculated GC between all hippocampal channels and all scalp EEG electrodes. We present here the electrode pairs with the highest ΔGranger values. It turned out that in each participant, the highest GC occurred in temporal electrodes over auditory cortex; in participants where temporal sites were not recorded from, the highest GC occurred at the neighboring electrode sites C3 or C4.

The GC time-course in Participant 1 was similar for scalp EEG (**Fig. 4 a**) and ECoG (**Fig. 2 e**). We found high GC between temporal EEG over auditory cortex (EEG site T4) and hippocampus. The GC was lower than for ECoG, as expected for

the lower signal amplitude of scalp EEG. During encoding, the information flow was from temporal EEG to hippocampus in the alpha frequency range (dark blue curve). During maintenance, the information flow range was reversed (dark red curve), i.e. from hippocampus to auditory cortex. In Participant 2, the information flow was high from electrode T5 to hippocampus during encoding in the alpha range (dark green line in **Fig. 4 b**). In Participant 3, the information flow was highest from hippocampus to electrode T6 during maintenance in the theta range (dark red line in **Fig. 4 c**). Also for all other participants (**Fig. 4 d-o**), all GC spectra during encoding had frequency ranges where information flow from cortex to hippocampus (encoding, dark blue curve) was significantly higher than in the reverse direction (light blue curve) and where information flow from hippocampus to cortex (maintenance, dark red curve) was significantly higher than in the reverse direction (light red curve). We then calculated the time-frequency plots of the ΔGranger for each participant; the averaged plot illustrates the predominant flow from auditory cortex to hippocampus during encoding (blue) and flow from hippocampus to auditory cortex (red) during maintenance in the theta-alpha frequency range (4-15 Hz, **Fig. 5a**).

Finally, we looked at the effect of behavior on ΔGranger. For each participant we calculated the ΔGranger for encoding and maintenance in the respective frequency bands of significance. For correct trials, the ΔGranger was negative during encoding and positive during maintenance for all 15 participants ($P = 0.005$, paired cluster based permutation test, **Fig. 5 b**). For incorrect trials, the same analysis was not significant ($P = 0.0647$, paired cluster based permutation test, **Fig. 5 c**) for incorrect trials. This suggests that timely information flow, as indexed by GC, is relevant for producing a correct response.

DISCUSSION

Working memory (WM) describes our capacity to represent sensory input for prospective use. Our findings suggest that this cognitive function is subserved by bidirectional oscillatory interactions between the hippocampus and the sensory-parietal cortex as indicated by phase synchrony and Granger causality. In our verbal working memory task, the encoding of letter items is isolated from the maintenance period in which the active rehearsal of memory items is central to achieve correct performance. First, analysis of task-induced power showed sustained oscillatory

activity in cortical and hippocampal sites during the maintenance period. Second, analysis of the inter-electrode phase synchrony and the directional information flow showed task-induced interactions between cortical and hippocampal sites. The oscillations were in the beta band when recorded with intracranial electrodes and, when recorded with scalp electrodes, extended down to the theta-alpha band. Third, the directional information flow was from sensory cortex to hippocampus during encoding and, during maintenance, the reverse flow occurred from hippocampus to cortex. Fourth, the comparison between correct and incorrect trials suggests that the participants relied on timely information flow to produce a correct response. Our data suggests a surprisingly simple model of information flow within a network that involves sensory cortices and hippocampus (**Fig. 5 d**): During encoding, letter strings are verbalized as melody. The incoming information flows from sensory cortex to hippocampus (bottom-up). During maintenance, participants actively recall and rehearse the melody. The Granger causality indicates the information flow from hippocampus to cortex (top-town) as the physiological basis for the replay of the memory items, which finally guides action.

The current study is embedded in previous studies using the same or similar tasks. Persistent firing of hippocampal neurons indicated hippocampal involvement in the maintenance of memory items (19-21). Parietal generators of theta-alpha EEG indicated involvement of parietal cortex in WM maintenance (3, 5, 7, 19, 27). The hippocampo-cortical phase synchrony (PLV) was high during maintenance of the high workload trials (19). Building on these previous studies, the current study focused on high workload trials and extended them by the analysis of directional information flow.

In the literature, there are several studies investigating the WM network. However, only few report directional interactions. One of these (17), reports cross-spectral directionality between intracranial recordings in frontal cortex and the medial temporal lobe in theta frequencies. One study on episodic memory suggests directional information flow to and from hippocampus (28). Interestingly, our analyses with intracranial recordings from posterior cortex revealed the most salient findings in the beta frequencies, which is in line with hippocampal findings (15) and theoretical considerations (29). For scalp EEG, the frequencies of synchronisation found in the current study also included the theta-alpha frequencies, in line with

scalp EEG findings during WM tasks (4, 6) and other tasks (26) that activate oscillations in long-range recurrent connections (24, 25).

In sum, these results corroborated earlier findings on the working memory network and extended them by providing a physiological mechanism for the active replay of memory items.

METHODS

Task

We used a modified Sternberg task in which the encoding of memory items and their maintenance were temporally separated (**Fig. 1a**). Each trial started with a fixation period ([−6, −5] s), followed by the stimulus ([−5, −3] s). The stimulus consisted of a set of eight consonants at the center of the screen. The middle four, six, or eight letters were the memory items, which determined the set size for the trial (4, 6, or 8 respectively). The outer positions were filled with "X," which was never a memory item. The participants read the letters and heard them spoken at the same time. After the stimulus, the letters disappeared from the screen, and the maintenance interval started ([−3, 0] s). A fixation square was shown throughout fixation, encoding, and maintenance. After maintenance, a probe was presented. The participants responded with a button press to indicate whether the probe was part of the stimulus. The participants was instructed to respond as rapidly as possible without making errors. After the response, the probe was turned off, and the participants received acoustic feedback regarding whether the response was correct or incorrect. The participants performed sessions of 50 trials in total, which lasted approximately 10 min each. Trials with different set sizes were presented in a random order, with the single exception that a trial with an incorrect response was always followed by a trial with a set size of 4. The task can be downloaded at www.neurobs.com/ex_files/expt_view?id=266.

Participants

The participants in the study were patients with drug resistant focal epilepsy. To investigate a potential surgical treatment of epilepsy, the patients were implanted with intracranial electrodes. The participants provided written informed consent for the study, which was approved by the institutional ethics review board (PB 2016-

02055). The participants had normal or corrected-to-normal vision. For nine participants (4 – 13), the PSD and PLV has been reported in an earlier study (19).

Electrodes for sEEG, ECoG, and EEG

The depth electrodes (1.3 mm diameter, 8 contacts of 1.6 mm length, spacing between contact centers 5 mm, ADTech®, Racine, WI, www.adtechmedical.com) were stereotactically implanted into the hippocampus. Subdural grids and strips were placed directly on the cortex according to the findings of the non-invasive presurgical evaluations. Platinum electrodes with 4 mm^2 contact surface and 1 cm inter-electrode distances were used (ADTech®). In addition, scalp EEG electrodes were placed at the sites of the 10-20 system with minor adaptations to avoid surgical scalp lesions.

Electrode localization

To localize the ECoG grids and strips, we used the participants' postoperative MR, aligned to CT and produced a 3D reconstruction of the participants' pial brain surface. Grid/strip electrode coordinates were projected on the pial surface as described in (30) (**Fig. 2a, Fig. 3a,f**).

The stereotactic sEEG electrodes were localized using post-implantation computed tomography (CT) and post-implantation structural T1- weighted MRI scans. The CT scan was registered to the post-implantation scan as implemented in FieldTrip (31). A fused image of CT and MRI scans was produced and the electrode contacts were marked visually. The contact positions were projected on a parasagittal plane of MRI (**Fig. 1b**).

Recording setup, re-referencing, and preprocessing

All recordings were performed with Neuralynx ATLAS, sampling rate 4000 Hz, 0.5-1000 Hz passband (Neuralynx, Bozeman MT, USA, www.neuralynx.com). ECoG and sEEG were recorded against a common intracranial reference. ECoG was then re-referenced against a sEEG contact in white matter. For each sEEG electrode, hippocampal contacts were re-referenced against their closest sEEG contact in white matter. The scalp EEG was recorded against an electrode near the vertex and was then re-referenced to the averaged mastoid channels. All signals were downsampled to 500 Hz. Trials with large unitary artefacts in the scalp EEG were rejected. We

focused on trials with high workload (set sizes 6 and 8) for further analysis. We used the FieldTrip toolbox for data processing and analysis (32).

Power spectral density

We first calculated the relative power spectral density (PSD) in the time-frequency domain (**Fig. 2 b**). Time-frequency maps for all trials were averaged. We used 3 multitapers with a window width of 10 cycles per frequency point, smoothed with 0.2 × frequency. We computed power in the frequency range 4-100 Hz with a time resolution of 0.1 s. The PSD during fixation ([−6.0, −5.0] s) served as a baseline for the baseline correction (PSD(t) – PSD(fixation))/ PSD(fixation) for each time-frequency point.

Phase locking value

To evaluate the functional connectivity of hippocampus and cortex, we calculated the phase-locking value (PLV) between hippocampal sEEG channels and ECoG grid (multitaper frequency transformation with 2 tapers based on Fourier transform, frequency range 4-100 Hz with frequency resolution of 1 Hz).

$$PLV_{i,j}(f) = \frac{1}{N}\left|\sum_{n=1}^{N}\frac{X_i(f)\cdot(X_j(f))^*}{|X_i(f)|\cdot|X_j(f)|}\right|$$

where $PLV_{i,j}$ is the PLV between channels i,j, N is the number of trials, X(f) is the Fourier transform of x(t), and $(\cdot)^*$ represents the complex conjugate.

Using the spectra of the two-second epochs, phase differences were calculated for each electrode pair (i,j) to quantify the inter-electrode phase coupling. The phase difference between the two signals indexes the coherence between each electrode pair and is expressed as the PLV. The PLV ranges between 0 and 1, with values approaching 1 if the two signals show a constant phase relationship over all trials.

In our description of EEG frequency bands, we used theta (4-8 Hz), alpha (8-12 Hz), beta (12-24 Hz) and gamma (> 40 Hz), while the exact frequencies may differ in individual participants.

Spectral Granger causality

In order to evaluate the direction of information flow between the hippocampus and the cortex, we calculated spectral non-parametric Granger causality (GC) as a measure of directed functional connectivity. GC examines if the activity on one channel can forecast activity in the target channel. In the spectral domain, GC

measures the fraction of the total power that is contributed by the source to the target. We transformed signals to the frequency domain using the multitaper method (2 tapers, frequency range 4 to 100 Hz with frequency resolution of 0.5 Hz, ± 2 Hz smoothing) to reduce spectral leakage and control the frequency smoothing.

We used a non-parametric spectral approach to measure the interaction in the channel pairs at a given interval time (33). In this approach, the spectral transfer matrix is obtained from the Fourier transform of the data. We used the FieldTrip toolbox to factorize the transfer function $\mathrm{H(f)}$ and the noise covariance matrix Σ. The transfer function and the noise covariance matrix was then employed to calculate the total and the intrinsic power, $\mathrm{S(f)} = \mathrm{H(f)\Sigma H^{*}(f)}$, through which we calculated the Granger interaction in terms of power fractions contributed from the source to the target.

$$GC_{Y\rightarrow X} \rightarrow= ln\frac{S_{xx(f)}}{\tilde{S}_{xx(f)}}$$

where $S_{xx(f)}$ is the total power and $\tilde{S}_{xx(f)}$ the instantaneous power. To improve legibility, we present GC as Granger % = GC*100 (**Fig. 2 d,e)**.

To illustrate the time course of GC over time, we calculated time-frequency maps for the selected pairs with scalp channels and averaged these maps over participants.

Statistics

To analyze statistical significance, we used cluster-based nonparametric permutation tests. To assess the significance of PLV and GC, we compared the true values to a null distribution. We recomputed GC after shuffling the trial number for a single channel in the pair, while keeping the trial number of the other channel constant. We repeated this n = 200 times to create a null distribution of GC. The null distribution was exploited to calculate the percentile threshold P = 0.05. We mark the frequency range of significant GC with a blue bar for encoding (dark blue spectrum exceeds light blue spectrum, information flow from cortex to hippocampus) and with a red bar for maintenance (dark red spectrum exceeds light red spectrum, information flow from hippocampus to cortex).

For comparisons between two groups, we used the paired cluster based permutation test. We created a null distribution by performing N = 200 random permutations. The significance threshold was established at P = 0.05.

Acknowledgments

We thank the physicians and the staff at Schweizerische Epilepsie-Klinik for their assistance and the patients for their participation. We acknowledge grants awarded by the Swiss National Science Foundation (SNSF 320030_176222 to J. S.) and SNSF Ambizione fellowship (PZ00P3_167836 to P. M.). The funders had no role in the design or analysis of the study.

Author contributions: J.S. designed the experiments. J.S. performed the experiments. V.D. and J.S. analyzed the data. L.S. performed surgery. P.M. visualized the grid electrode position, V.D. and J.S. wrote the manuscript. All of the authors reviewed the final version of the manuscript.

Competing interests: All authors declare that they have no competing interests.

Ethical considerations: The participant provided written informed consent for the study, which was approved by the institutional ethics review board (PB 2016-02055).

Data availability: All data needed to evaluate the conclusions in the paper are present in the paper. The task can be downloaded at www.neurobs.com/ex_files/expt_view?id=266. The raw data will be made publicly available after acceptance of the manuscript.

FIGURE CAPTIONS

Figure 1. Task and recording sites.

a) In the task, sets of consonants are presented and have to be memorized. The set size (4, 6 or 8 letters) determines WM workload. In each trial, presentation of a letter string (encoding period, 2 s) is followed by a delay (maintenance period, 3 s). After the delay, a probe letter is presented. Participants indicate whether the probe was in the letter string or not.

b) Response accuracy decreases with set size (71 sessions).

c) Reaction time increases with set size (53 ms/item).

d) The tip locations of the hippocampal sEEG electrodes for all participants (N = 15) are projected on the parasagittal plane x = 25.2 mm.

Figure 2. Encoding and replay of letters in Participant 1

a) Location of the ECoG contacts over temporal and parietal cortex for Participant 1. Contacts record from auditory cortex (C2, cyan) and occipital-parietal cortex (H3, magenta).

b) The relative power spectral density (PSD) in the parietal contact (magenta) shows gamma (>40 Hz) during encoding [-5 -3] s while the subject sees and hears the letters. Sustained beta activity (11-14 Hz) appears towards the end of the maintenance period [-3 0] s.

c) Hippocampal PSD shows sustained beta activity towards the end of maintenance.

d) Phase locking value (PLV) between cortex and hippocampal sEEG in beta during maintenance. PLV (16-29 Hz) is maximal in contact C2 over auditory cortex.

e) Spectral Granger causality. During encoding, auditory cortex (contact C2) predicts hippocampus (8-18 Hz, dark blue curve exceeds light blue curve). During maintenance, hippocampal sEEG predicts auditory cortex (8-14 Hz, dark red curve exceeds light red curve).

f) The Granger time-frequency map illustrates the spectra of panel e. During encoding, net information (ΔGranger) starts to flow from auditory cortex to hippocampus (blue). During maintenance the information flow is reversed from hippocampus to auditory cortex (red) indicating the replay of letters in memory.

Figure 3. Encoding and replay of letters in two participants with ECoG

a) Location of the ECoG contacts in Participant 2. The most anterior strip contact (cyan) records from auditory cortex.

b) The relative power spectral density (PSD) in the temporal scalp EEG electrode (T3) shows beta (14-25 Hz) during encoding [-5 -3] s while the subject sees and hears the letters. Sustained theta activity (6-9 Hz) appears towards the end of the maintenance period [-3 0] s.

c) Hippocampal PSD shows sustained alpha-beta activity (9-21 Hz) towards the end of maintenance.

d) Spectral Granger causality. During encoding, the auditory cortex predicts hippocampus (9-16 Hz, dark blue curve exceeds light blue curve). During maintenance, hippocampal sEEG predicts auditory cortex (9-16 Hz, dark red curve exceeds light red curve).

e) The time-frequency map illustrates the time course of ΔGranger in Participant 3.
f) Location of the ECoG contacts in Participant 3. The most posterior contact (cyan) records from visual cortex.
g) The relative power spectral density (PSD) in the blue contact shows gamma during encoding while the subject sees the letters. Sustained alpha activity (7-12 Hz) appears towards the end of the maintenance period.
h) Hippocampal PSD shows sustained beta activity (13-22 Hz) towards the end of maintenance.
i) Spectral Granger causality. During encoding, the occipital ECoG (cyan contact) predicts hippocampus (10-18 Hz, dark blue curve exceeds light blue curve). During maintenance, hippocampal sEEG predicts ECoG (9-18 Hz, dark red curve exceeds light red curve).
j) The time-frequency map illustrates the time course of ΔGranger in Participant 3.
Bars: frequency range of significant ΔGranger ($p<0.05$), cluster-based nonparametric permutation test against a null distribution with scrambled trials during encoding (dark blue) and maintenance (dark red), respectively.

Figure 4. Granger causality between hippocampal sEEG and scalp EEG

Granger causality spectra for hippocampal sEEG and scalp EEG for the electrode pair with maximal Granger causality for all participants (N=15). During encoding, the net Granger (ΔGranger) indicates information flow from scalp EEG to hippocampal sEEG (blue bar). During maintenance, ΔGranger indicates information flow from hippocampal sEEG to scalp EEG to (red bar). Each panel carries the name of the scalp EEG electrode site.
Bars: frequency range of significant ΔGranger ($p<0.05$), cluster-based nonparametric permutation test against a null distribution with scrambled trials during encoding (dark blue) and maintenance (dark red), respectively. Colors of Granger spectra indicating information flow:
dark blue, EEG to hippocampus during encoding;
light blue, hippocampus to EEG during encoding;
dark red, hippocampus to EEG during maintenance;
light red, EEG to hippocampus during maintenance.

Figure 5. Information flow in the working memory network relates to behavior.

a) The time-frequency map of net Granger causality (ΔGranger), averaged over all N=15 participants, illustrates the time course of the information flow from scalp EEG to hippocampus (blue) during encoding and from hippocampus to scalp EEG (red) during maintenance.

b) For correct trials, the maximal ΔGranger is negative during encoding (blue, cortex → hippocampus) and positive during maintenance (red, hippocampus → cortex) for all participants (triangles: pairs with scalp EEG, circles: pairs with ECoG, P = 0.005, paired cluster based permutation test).

c) For incorrect trials, the maximal ΔGranger is highly variable (P = 0.0647, paired cluster based permutation test, not significant).

d) Bidirectional information flow between posterior cortical sites and hippocampus in the working memory network. The data suggest a surprisingly simple model of information flow during the task. During encoding, letter strings are verbalized as a melody. The incoming information flows from sensory cortex to hippocampus. During maintenance, participants actively recall and rehearse the melody. The Granger causality indicates the information flow from hippocampus to cortex as the physiological basis for the replay of the memory items.

Figure S1. Further analyses in Participant 1

a) The relative power spectral density (PSD) in the temporal contact (grid contact C2, cyan in Figure 2 a) shows gamma (>40 Hz) during encoding [-5 -3] s while the subject sees and hears the letters, thus confirming the anatomical location of this contact over auditory cortex.

b) Phase locking value (PLV) between hippocampus and grid contact C2. To assess the significance of the difference of the PLV between different task periods, we used the same permutation test as for the evaluation of significance for Granger causality. We mark the frequency range of significant PLV (18-30 Hz) with a red bar when the PLV spectrum during maintenance (red spectrum) exceeds the PLV spectrum during fixation (black spectrum).

c) Spectral Granger causality during encoding. In the 8-18 Hz range, auditory cortex (contact C2) is maximal in predicting hippocampus.

d) Spectral Granger causality during maintenance. In the 8-14 Hz range, hippocampus predicts auditory cortex (contact C2) and parietal cortex (contact F7). Axis labels denote contact names.

REFERENCES

1. Baddeley A (2003) Working memory: looking back and looking forward. *Nat Rev Neurosci* 4(10):829-839.
2. Christophel TB, Klink PC, Spitzer B, Roelfsema PR, & Haynes J-D (2017) The Distributed Nature of Working Memory. *Trends in Cognitive Sciences* 21(2):111-124.
3. Michels L, Moazami-Goudarzi M, Jeanmonod D, & Sarnthein J (2008) EEG alpha distinguishes between cuneal and precuneal activation in working memory. *NeuroImage* 40(3):1296-1310.
4. Sarnthein J, Petsche H, Rappelsberger P, Shaw GL, & von Stein A (1998) Synchronization between prefrontal and posterior association cortex during human working memory. *Proc Natl Acad Sci U S A* 95(12):7092-7096.
5. Tuladhar AM*, et al.* (2007) Parieto-occipital sources account for the increase in alpha activity with working memory load. *Hum Brain Mapp* 28(8):785-792.
6. Polania R, Nitsche MA, Korman C, Batsikadze G, & Paulus W (2012) The importance of timing in segregated theta phase-coupling for cognitive performance. *Curr Biol* 22(14):1314-1318.
7. Näpflin M, Wildi M, & Sarnthein J (2008) Test-retest reliability of EEG spectra during a working memory task. *NeuroImage* 43(4):687-693.
8. Bidelman GM, Brown JA, & Bashivan P (2021) Auditory cortex supports verbal working memory capacity. *Neuroreport* 32(2):163-168.
9. Pavlov YG & Kotchoubey B (2020) Oscillatory brain activity and maintenance of verbal and visual working memory: A systematic review. *Psychophysiology*:e13735.
10. Cogan GB*, et al.* (2017) Manipulating stored phonological input during verbal working memory. *Nat Neurosci* 20(2):279-286.
11. Raghavachari S*, et al.* (2001) Gating of human theta oscillations by a working memory task. *J Neurosci* 21(9):3175-3183.
12. Rizzuto DS*, et al.* (2003) Reset of human neocortical oscillations during a working memory task. *Proceedings of the National Academy of Sciences* 100(13):7931-7936.
13. Maris E, van Vugt M, & Kahana M (2011) Spatially distributed patterns of oscillatory coupling between high-frequency amplitudes and low-frequency phases in human iEEG. *NeuroImage* 54(2):836-850.
14. van Vugt MK, Schulze-Bonhage A, Litt B, Brandt A, & Kahana MJ (2010) Hippocampal gamma oscillations increase with memory load. *J Neurosci* 30(7):2694-2699.
15. Leszczyński M, Fell J, & Axmacher N (2015) Rhythmic Working Memory Activation in the Human Hippocampus. *Cell Rep* 13(6):1272-1282.
16. Schwiedrzik CM*, et al.* (2018) Medial prefrontal cortex supports perceptual memory. *Current Biology* 28(18):R1094-R1095.

17. Johnson EL, *et al.* (2018) Dynamic frontotemporal systems process space and time in working memory. *PLOS Biology* 16(3):e2004274.
18. Johnson EL, *et al.* (2019) Spectral Imprints of Working Memory for Everyday Associations in the Frontoparietal Network. *Front Syst Neurosci* 12:65.
19. Boran E, *et al.* (2019) Persistent hippocampal neural firing and hippocampal-cortical coupling predict verbal working memory load. *Sci Adv* 5(3):eaav3687.
20. Kamiński J, *et al.* (2017) Persistently active neurons in human medial frontal and medial temporal lobe support working memory. *Nat Neurosci* 20(4):590-601.
21. Kornblith S, Quian Quiroga R, Koch C, Fried I, & Mormann F (2017) Persistent Single-Neuron Activity during Working Memory in the Human Medial Temporal Lobe. *Curr Biol* 27(7):1026-1032.
22. Rutishauser U, Reddy L, Mormann F, & Sarnthein J (2021) The Architecture of Human Memory: Insights from Human Single-Neuron Recordings. *The Journal of Neuroscience* 41(5):883-890.
23. Hsieh LT & Ranganath C (2014) Frontal midline theta oscillations during working memory maintenance and episodic encoding and retrieval. *NeuroImage* 85 Pt 2:721-729.
24. Fries P (2015) Rhythms for Cognition: Communication through Coherence. *Neuron* 88(1):220-235.
25. Pesaran B, *et al.* (2018) Investigating large-scale brain dynamics using field potential recordings: analysis and interpretation. *Nat Neurosci* 21(7):903-919.
26. Solomon EA, *et al.* (2017) Widespread theta synchrony and high-frequency desynchronization underlies enhanced cognition. *Nat Commun* 8(1):1704.
27. Boran E, *et al.* (2020) Dataset of human medial temporal lobe neurons, scalp and intracranial EEG during a verbal working memory task. *Sci Data* 7(1):30.
28. Griffiths BJ, *et al.* (2019) Directional coupling of slow and fast hippocampal gamma with neocortical alpha/beta oscillations in human episodic memory. *Proc Natl Acad Sci U S A* 116(43):21834-21842.
29. Gelastopoulos A, Whittington MA, & Kopell NJ (2019) Parietal low beta rhythm provides a dynamical substrate for a working memory buffer. *Proc Natl Acad Sci U S A* 116(33):16613-16620.
30. Groppe DM, *et al.* (2017) iELVis: An open source MATLAB toolbox for localizing and visualizing human intracranial electrode data. *J Neurosci Methods* 281:40-48.
31. Stolk A, *et al.* (2017) Integrated analysis of anatomical and electrophysiological human intracranial data. *bioRxiv*.
32. Oostenveld R, Fries P, Maris E, & Schoffelen J-M (2011) FieldTrip: Open Source Software for Advanced Analysis of MEG, EEG, and Invasive Electrophysiological Data. *Computational Intelligence and Neuroscience* 2011:9.
33. Bastos AM & Schoffelen J-M (2016) A Tutorial Review of Functional Connectivity Analysis Methods and Their Interpretational Pitfalls. *Frontiers in systems neuroscience* 9:175-175.

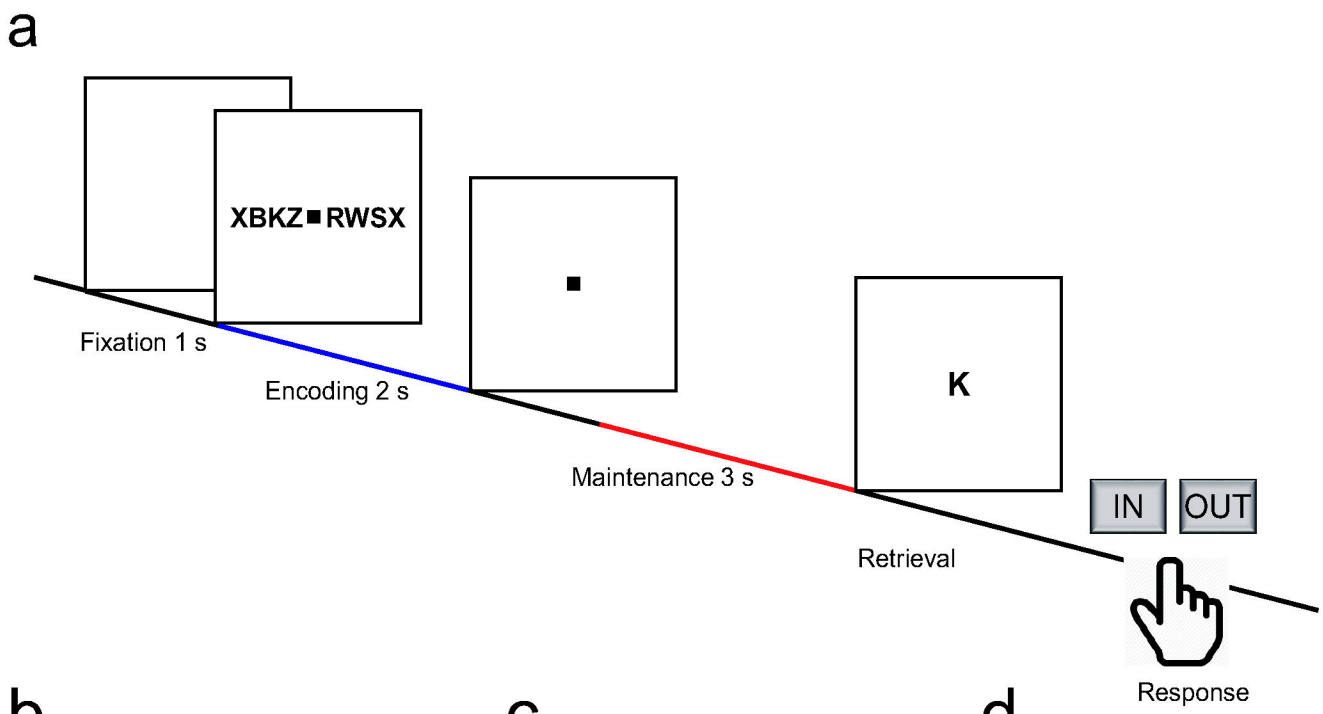

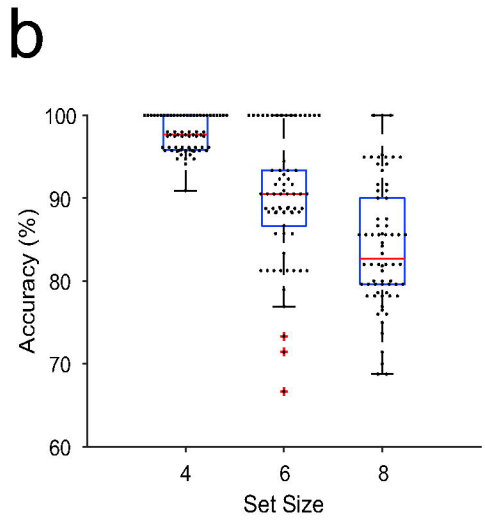

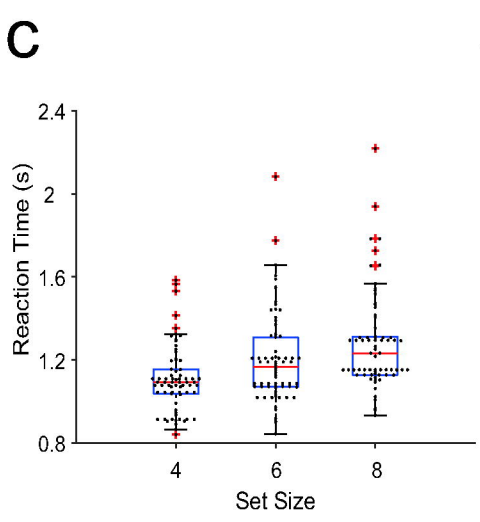

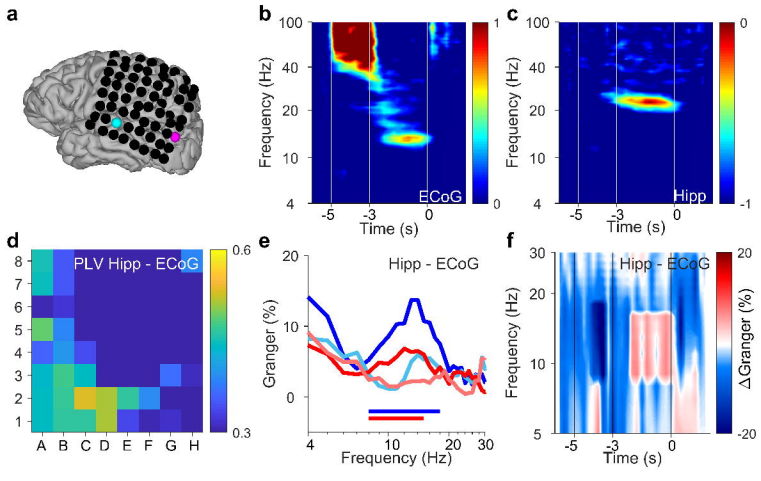
a
b
Frequency (Hz)
100
40
20
10
4
-5
-3
0
Time (s)
ECoG
1
0
c
Frequency (Hz)
100
40
20
10
4
-5
-3
0
Time (s)
Hipp
0
-1
d
PLV Hipp - ECoG
8
7
6
5
4
3
2
1
A B C D E F G H
0.6
0.3
e
Hipp - ECoG
Granger (%)
20
10
0
4
10
20
30
Frequency (Hz)
f
Hipp - ECoG
Frequency (Hz)
30
20
10
5
-5
-3
0
Time (s)
ΔGranger (%)
20
-20

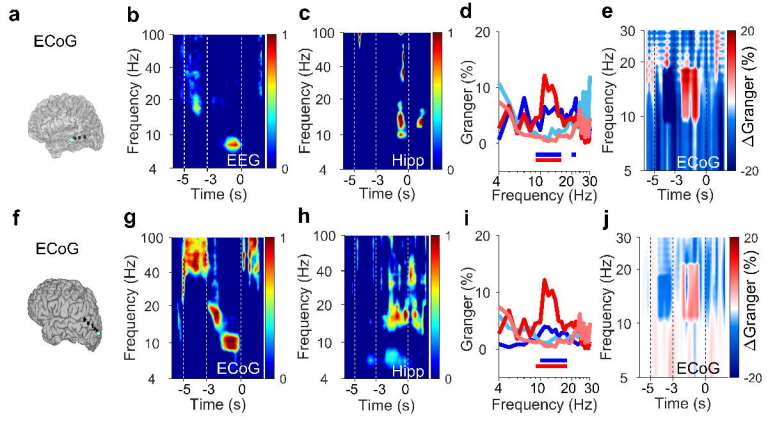
a
ECoG
b
Frequency (Hz)
100
40
20
10
4
EEG
-5
-3
0
Time (s)
1
0
c
Frequency (Hz)
Hipp
d
Granger (%)
20
10
0
4
10
20
30
Frequency (Hz)
e
Frequency (Hz)
30
20
10
5
ECoG
ΔGranger (%)
f
ECoG
g
ECoG
h
Hipp
i
j

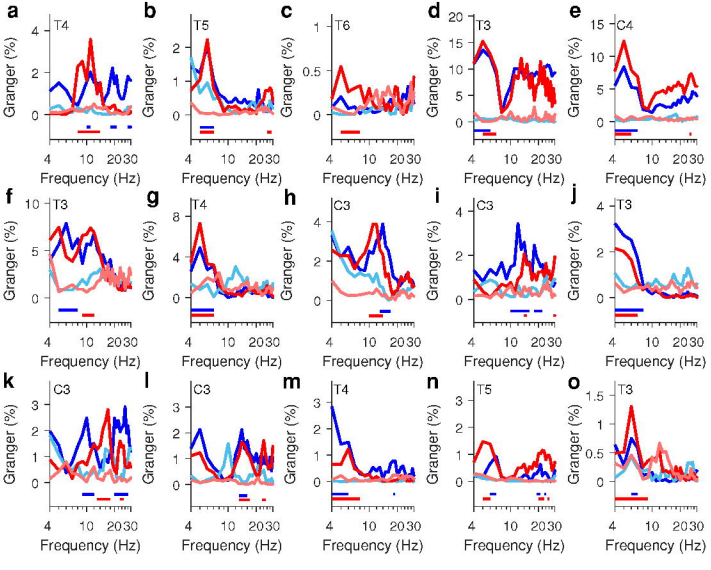
a
T4
b
T5
c
T6
d
T3
e
C4
f
T3
g
T4
h
C3
i
C3
j
T3
k
C3
l
C3
m
T4
n
T5
o
T3
Granger (%)
Frequency (Hz)
4
10
20
30